High-efficiency backlight module with two guiding modes

Chang-Yi Li[1] and Jui-Wen Pan[1,2,3,*]

[1]Institute of Photonics System, National Chiao Tung University, Tainan City 71150, Taiwan

[2]Department of Medical Research, Chi Mei Medical Center, Tainan City 71004, Taiwan

[3]Biomedical Electronics Translational Research Center, National Chiao Tung University, Hsin-Chu City 30010, Taiwan

*Corresponding author: juiwenpan@gmail.com

Received 12 November 2013; revised 23 January 2014; accepted 28 January 2014;
posted 29 January 2014 (Doc. ID 201115); published 4 March 2014

We propose a design for a high-efficiency backlight module that does not require a brightness enhancement film (BEF). With the high-efficiency backlight module it is possible to achieve almost the same half-luminance angle as a conventional edge-lit backlight module can achieve. The backlight system is comprised of a crisscross light guide plate (LGP) and one diffuser sheet. The crisscross LGP is composed of a LGP and optically patterned film (OPF). The backlight module allows light to be extracted through the direct guiding mode and top guiding mode, respectively. We controlled arrangement of the microstructures to increase the optical efficiency and the uniformity by two modes. Compared to the conventional edge-lit backlight module, there is a two-fold improvement in both the total optical efficiency and on-axis luminance with the high-efficiency backlight module.

OCIS codes: (150.2945) Illumination design; (220.4830) Systems design; (350.3950) Micro-optics; (230.3670) Light-emitting diodes; (230.4000) Microstructure fabrication.

http://dx.doi.org/10.1364/AO.53.001503

1. Introduction

The LED recently has become the main light source used in backlight modules because it offers low-power dissipation, high robustness, a small form factor, and good efficiency [1,2]. For these reasons, LED backlight module design has progressed rapidly. However, there is a loss of the light energy of approximately 49% from the light source to the backside of the LCD, which means the optical efficiency of the backlight module is very low [3]. The energy loss of the backlight module can be determined by taking into account the absorption of the materials, plus the light scattering and consumption of the optical film [4]. In a conventional edge-lit backlight module, two brightness enhancement films (BEFs) must be used to enhance the brightness of the backlight module [5]. However, these optical films can increase the Fresnel reflections. Thus, many investigators have proposed a microstructural design for the light guide plate (LGP) [6–8]. This solution not only increases the optical efficiency but also can reduce the need for optical films in the backlight system. Determining how to increase the light efficiency of the liquid crystal display has become a major issue.

Currently, the flow-line theory is the basis for the most powerful method for enhancing the efficiency of the backlight module. The light is guided through the LGP by the total internal reflection, so it is possible to achieve a very high optical efficiency [9]. Using the flow-line method, it is possible to not only calculate the angle of the microstructures, but also construct the architecture of the LGP. However, the shape is difficult to calculate [10]. By considering the manufactured microstructures with round angles, an optical efficiency of 61.2% can be achieved. Proper flow lines between the top guide line and the guide

1559-128X/14/081503-09$15.00/0

segments are needed, however, and alignment problems can exist when the LGP is designed based on flow-line theory.

In this study, the backlight system under consideration is comprised of a crisscross LGP and one diffuser sheet. The crisscross LGP is composed of an LGP and optically patterned film (OPF). The OPF is in direct contact with the LGP, secured by a photo-curable adhesive, so that light rays can propagate directly through the optical window [11,12]. The LGP's upper surface is patterned with prism-shaped microstructures. The top and bottom surface of the OPF also are both patterned with microstructures. The light is collimated in the horizontal direction by the top microstructures of the OPF while the bottom microstructures ensure collimation of the rays in the vertical direction. Thus, the OPF replaces the function of the crossed BEFs. A crisscross LGP with simple prism microstructures is designed and simulated using the LightTools software. The tolerance for the round angle of the prism microstructures manufactured by the injection process is analyzed. Not only does this design achieve an optical efficiency of 64.7%, but an illumination uniformity of 91.4% also is obtained using the nine-point measuring method [13]. Tolerance analysis also is completed.

2. Working Principles of the Crisscross Light Guide Plate

A. Two-mode Light Extraction

When compared to the conventional edge-lit model, there is an enhancement of optical efficiency, as Fig. 1(a) shows. The conventional edge-lit backlight module comprises a reflector, a wedge-shaped LGP, a bottom diffuser, two BEFs, and a top diffuser [14–17]. The structure of the crisscross LGP with the LGP and OPF is shown in Fig. 1(b). One can see the prism microstructures on top of the LGP and the trapezoidal and prism microstructures on the top and bottom of the OPF. The trapezoidal microstructures are in contact with the bottom of the LGP, while the bottom of the OPF is coated with silver.

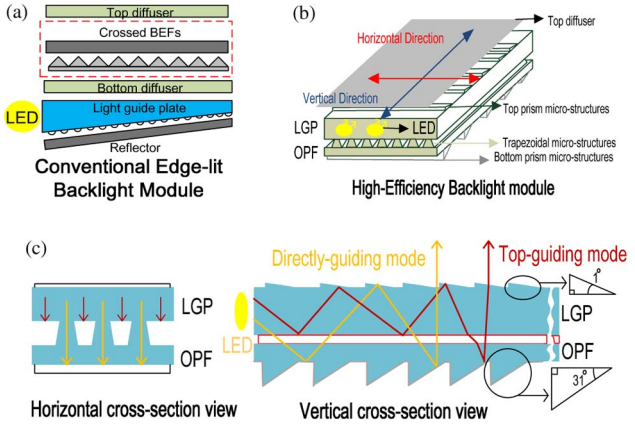

Fig. 1. Principles of the crisscross LGP: (a) architecture of the conventional edge-lit backlight module, (b) architecture of the high-efficiency backlight module, and (c) extracted light of the two modes.

There are two modes for light extraction, direct guiding and top guiding, as shown in Fig. 1(c). In the direct guiding mode, the light encounters the interface between the bottom of the LGP and trapezoidal microstructures of the OPF. The light passes directly through the trapezoidal microstructures to be reflected by the prisms on the bottom of the OPF. The density of the bottom prism microstructures can be adjusted to obtain uniform illumination. In the top guiding mode, light that does not hit the trapezoidal microstructures is guided by total internal reflection within the LGP. The light is deflected by the top prism microstructures. The light propagates through the air to the OPF, where it will be reflected by the bottom prism microstructures. The density of the top prism microstructures also can be adjusted to obtain uniform illumination. Since the slanted angle of the top prism microstructures is designed by only one degree, the direct guiding mode is almost unaffected by the top prism microstructures. The uniformity of the illumination for the crisscross LGP can be adjusted by changing the density of the prism-shaped microstructures at the bottom and the top. In other words, the design of the microstructures on the LGP and OPT can improve the light extraction efficiency, reducing the trapped light by the crisscross LGP. Using this approach, we can improve both the optical efficiency and illumination uniformity.

B. Working Principles for Designing the Trapezoid Microstructures in the Crisscross Light Guide Plate

The crisscross LGP includes the prism-shaped microstructures on the top, trapezoidal microstructures and bottom prism microstructures. A previous study showed how to ensure the collimation of light in the vertical dimension by the design of the bottom prism microstructures [18]. Pan *et al.* used a hybrid LGP for collimation of light in the vertical dimension [19]. In this study, the light can also be collimated in the horizontal dimension by the trapezoidal microstructures at the middle of the crisscross LGP, as shown in Fig. 2(a). Because the LGP and OPF are both fabricated from Polymethylmethacrylate (PMMA), it can be assumed they have the same refractive index and the étendue principle can be used for analysis [20].

According to this principle, the étendue is conserved as a cross-sectional area multiplied by the solid angle it subtends [21]. The top cross-sectional area of the microstructures is smaller than the bottom cross-sectional area. As a result, the solid angle Ω_2 is smaller than the solid angle Ω_1 as indicated by the green arrows in Fig. 2(a). When the light is reflected back to the microstructures, as shown by the red arrows in Fig. 2(a), the angle at which it hits them again means that the light cannot achieve the collimation effect. Therefore, the slanted angle of the microstructures must be designed to avoid the light

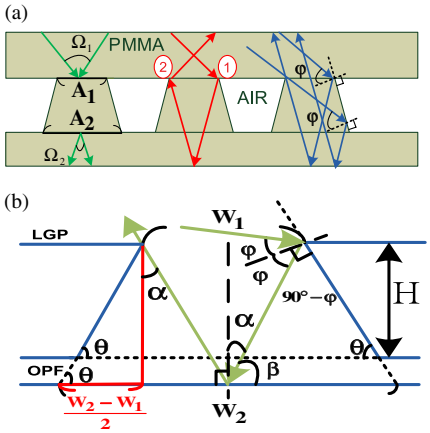

Fig. 2. Collimation principles for the crisscross light guide plate: (a) horizontal cross-sectional view of the crisscross light guide plate and (b) calculation of the slanted angle.

hitting them twice, as shown by the blue arrows in Fig. 2(a). If the incident angle is less than the critical angle, the incident light will penetrate the microstructures. The light path is too complex to calculate. For this reason, we use the critical angle to analyze collimation in the horizontal dimension. Based on the edge-ray principle, the edge ray at the critical angle φ enters the microstructures to be affected by total internal reflection [22]. The edge ray can exit successfully after it is reflected back. In other words, all incident light at the critical angle can be collimated in the horizontal dimension. In this design (blue arrows), the crisscross LGP is used to achieve the maximum optical efficiency.

When the light at the critical angle hits the highest position H on the microstructures, it will propagate through the bottom of the OPF. The light will then be reflected by the bottom of the OPF, which is coated with silver. Figure 2(b) shows a schematic representation. The relationship can be described as follows:

$$\beta = 180° - (90° - \varphi) - \theta, \tag{1}$$

$$\alpha = 90° - \beta = \theta - \varphi. \tag{2}$$

In this design, the bottom areas of the microstructures are twice as large as the top areas. The angle of the light can be described as follows:

$$W_2 = 2W_1, \tag{3}$$

$$\frac{W_2 - W_1}{2}\tan\theta = \frac{W_1}{2}\cot(\theta - \varphi), \tag{4}$$

$$\theta + \theta - \varphi = 2\theta - \varphi = 90°. \tag{5}$$

Based on Snell's law, the angle φ can be derived from Eq. (4), such that the angle θ will be calculated as in Eq. (8):

$$n_{\mathrm{PMMA}} \sin\varphi = n_{\mathrm{AIR}} \sin(90°), \tag{6}$$

$$\varphi = \sin^{-1}\left(\frac{1}{n_{\mathrm{PMMA}}}\right) \approx 42°, \tag{7}$$

$$\theta = \frac{90° + 42°}{2} = 66°. \tag{8}$$

The angle θ of the microstructures that will allow collimation of the light in the horizontal dimension can be determined from Eq. (8).

3. Optical Design and Simulation

A. High Uniformity and Improvement in Optical Efficiency by Two Guiding Modes

The high-efficiency backlight module is simulated using the LightTools software. In this model, 18 LEDs (Nichia NxSW155) are located around the edge of the LGP. A diffuser is added above the crisscross LGP to reduce the flaws. The size of the crisscross LGP is 10.1 inches (16:9). Table 1 shows the details about its thickness, materials, and the angle of the microstructures. Table 2 shows the exact sizes of the three kinds of microstructures.

In the direct guiding mode, illumination uniformity can be controlled by adjusting the density of the bottom prism microstructures, as shown in Fig. 3(a). The optical efficiency and illumination uniformity are obtained using LightTools. The illumination uniformity and optical efficiency of the backlight module are 85.3% and 57.9%, respectively. The prism microstructures are subsequently added to the top surface of the LGP, as shown in Fig. 3(b). In the top guiding mode, the density of the top prism microstructures can be adjusted to improve the illumination uniformity and optical efficiency.

The relationship between the x-directional position x and cover ratio α is shown in Fig. 3(c). The area of microstructures B can be calculated by Eq. (9), where $W(x)$ is the distribution function of the microstructures and L is the length of the microstructures. The cover ratio of the bottom prism microstructures can be evaluated by Eq. (10), where $W_{\mathrm{bottom}}(x)$ is the distribution function of the bottom prism microstructures and A is the area of the crisscross LGP.

Table 1. Simulated Conditions for Each Layer

Layer	Thickness (mm)	Material	Index	Position of Microstructures	Slanted angle of Microstructures (deg)
LGP	1.4	PMMA	1.49	Top	1
OPF	0.15	PMMA	1.49	Top	66
				Bottom	31

Table 2. Exact Sizes of Three Kinds of Microstructures

Name	Length of Microstructure (mm)	Height of Microstructure (μm)	Width of Microstructure (μm)
Top prism microstructures	226.60	0.87	50
Trapezoidal microstructures	125.70	22.46	Top 20 bottom 40
Bottom prism microstructures	226.60	18.03	30

$$B = \int_0^x L \times W(x)\mathrm{d}x, \tag{9}$$

$$\alpha\Big|_{W(x)=W_{\text{bottom}}} = \frac{B}{A}\Big|_{W(x)=W_{\text{bottom}}}. \tag{10}$$

The cover ratio of the top prism microstructures also can be derived by using Eq. (11), where

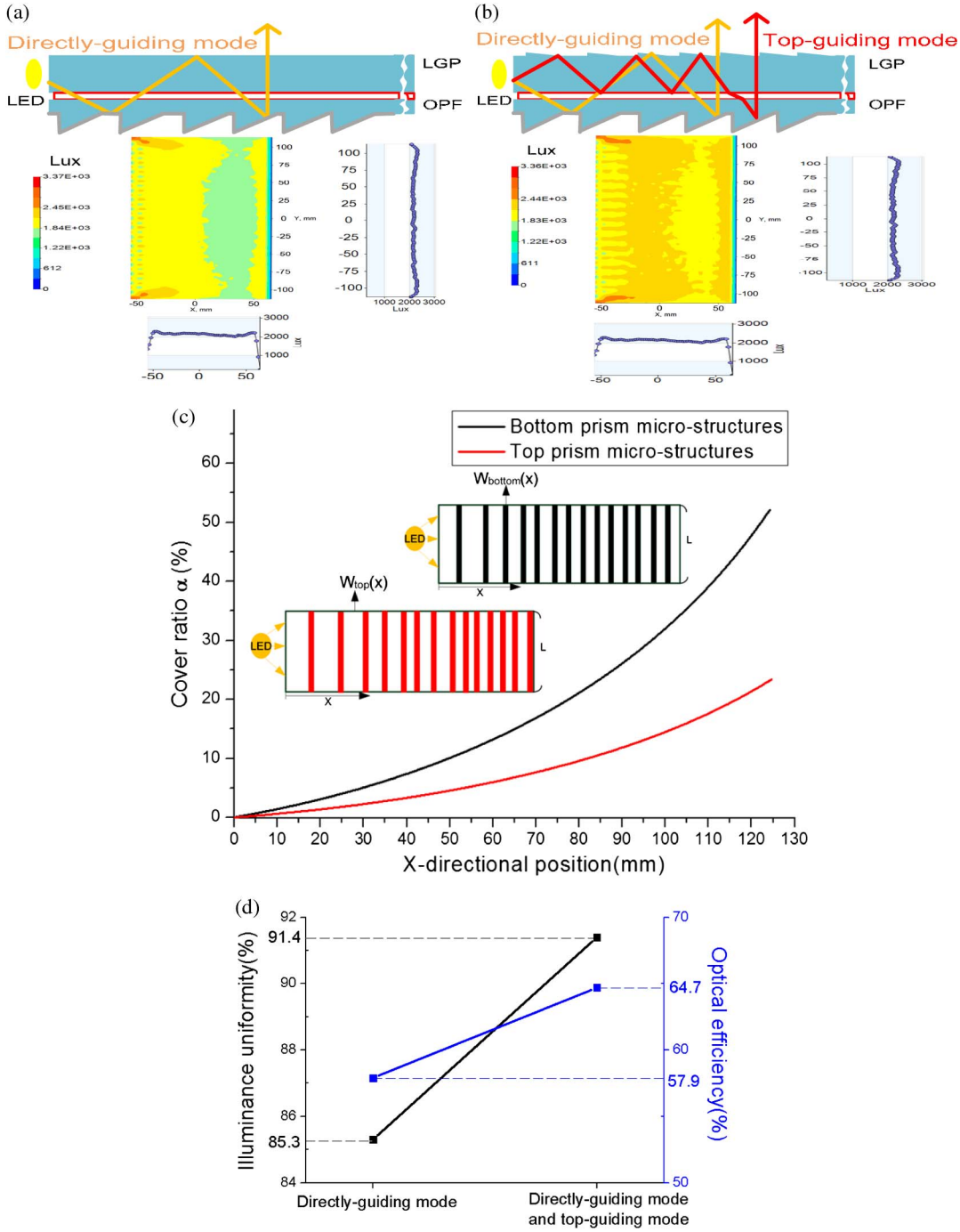

Fig. 3. Efficiency and uniformity of the high-efficiency backlight module: (a) illumination chart for the direct passing mode, (b) illumination chart for the two modes, (c) distribution of the top prism and bottom prism microstructures, and (d) efficiency and uniformity of the high-efficiency backlight module.

$W_{top}(x)$ is the distribution function of the top prism microstructures.

$$\alpha\Big|_{W(x)=W_{top}} = \frac{B}{A}\Big|_{W(x)=W_{top}}. \tag{11}$$

The optical efficiency and illumination uniformity in the direct guiding mode and top guiding mode can both be increased by optimizing the density of the prism microstructures. The relationship between efficiency and uniformity is shown in Fig. 3(d). The uniformity of the backlight module is increased to 91.4% and the efficiency is increased to 64.7%.

B. Relationship between the Optical Efficiency, Normalized On-axis Luminance and Density of the Trapezoidal Microstructures

The arrangement of the trapezoidal microstructures is periodical. Figure 4(a) shows the density of the trapezoidal microstructures as defined by Eq. (12), where density is represented by ρ, N is the number of trapezoidal microstructures and W is the width of the LGP. We can obtain the relationship between the optical efficiency, normalized on-axis luminance and density of the trapezoidal microstructures, as shown in Fig. 4(b). The normalized on-axis luminance is obtained from the on-axis luminance of the high-efficiency backlight module divided by the on-axis luminance of the conventional edge-lit backlight module:

$$\rho = \frac{N}{W}. \tag{12}$$

When the density of the trapezoidal microstructures is 0, the normalized on-axis luminance is 0.005. Because the light cannot enter the OPF, most of the light cannot be collimated. By increasing the density of the trapezoidal microstructures, more light can enter the OPF, leading to an increase in the normalized on-axis luminance and optical efficiency. For maximum optical efficiency, the density of the trapezoidal microstructures in our design is 12.5.

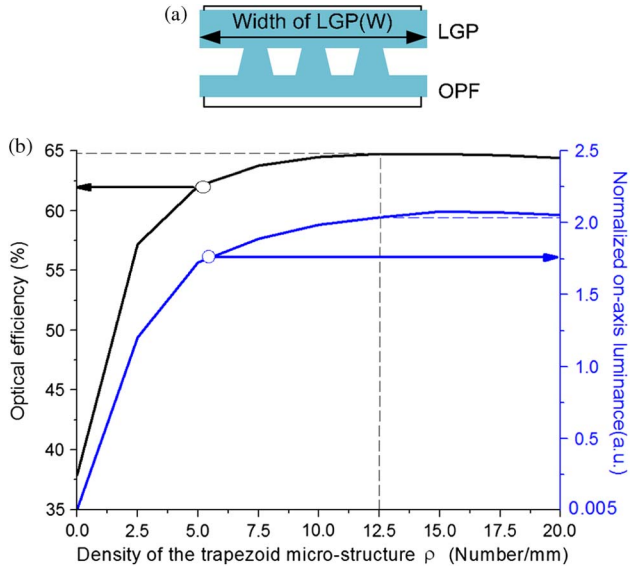

Fig. 4. Definition of the density of the trapezoid microstructures and the influence of the density on the optical efficiency and normalized on-axis luminance: (a) illumination chart for density; (b) relationship between the trapezoidal microstructures, optical efficiency, and normalized on-axis luminance.

C. Experimental Results and Loss Analysis

Figure 5 shows the relationship between the measured data and simulated data for the conventional edge-lit backlight module. In the measured data, the half-luminance angle is 20.5 deg while in the simulated data, the half-luminance angle is 22.5 deg. The results show that the measured data are similar to the simulated data for the conventional edge-lit backlight module, an indication of the reliability of the LightTools simulation.

In the simulation, loss analysis is more convenient than with real-world measurements. For loss analysis of the conventional edge-lit backlight module, we set five receivers on the top of the optical components and four edge leakage receivers surround the backlight module. The five receivers in different locations detect how much luminous flux can escape from the top of the optical components, as shown in Fig. 6(a). The four edge leakage receivers indicate the light leakage from the edge of the backlight module. For loss analysis of the high-efficiency backlight module, there are two receivers, one on top of the crisscross LGP and one on the diffuser, as shown in Fig. 6(b). There also are four edge leakage receivers surrounding the high-efficiency backlight module. Energy loss for the backlight module can be defined as in Eq. (13), where γ is the ratio of the energy loss of optical components. For the backlight module, α is the optical energy of the light emitting sources, the optical energy of four edge leakage receivers is represented by β and the optical energy of receiver 5 is represented by η:

$$\gamma(\%) = \left[\frac{(\alpha - \beta - \eta)}{\alpha}\right] \times 100\%. \tag{13}$$

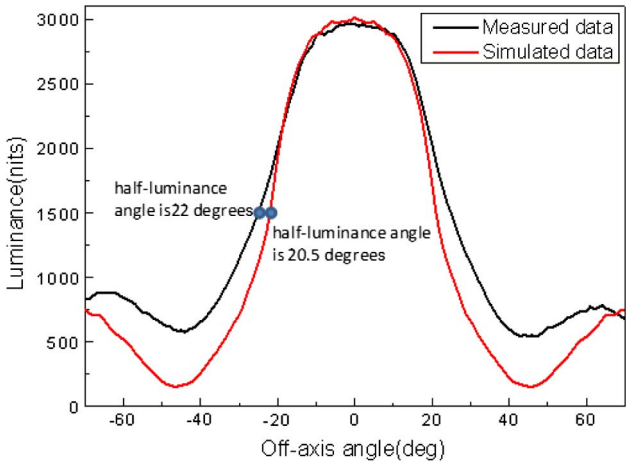

Fig. 5. Measured data and simulated data.

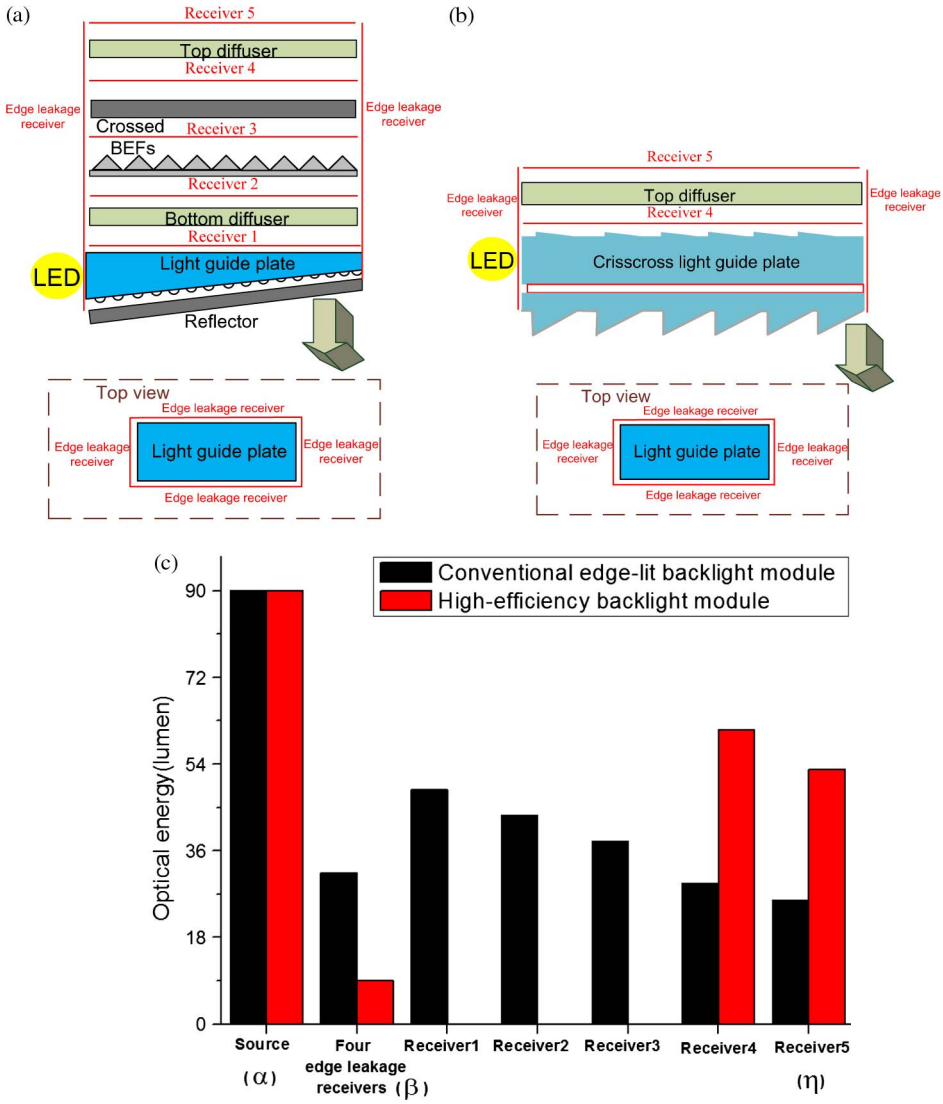

Fig. 6. Receiver settings and loss analysis in the two backlight modules: (a) receiver settings for the conventional edge-lit backlight module, (b) receiver settings for the high-efficiency backlight module, and (c) loss analysis for the conventional edge-lit backlight module and the high-efficiency backlight module.

The results of the optical simulation for the two backlight modules are shown in Fig. 6(c). Here, γ is 36.59% for the conventional edge-lit backlight module while for the high-efficiency backlight module, γ is 31.27%. The simulation results show the total energy at the four edge leakage receivers and energy loss of the optical components to be higher in the conventional edge-lit backlight module than in the high-efficiency backlight module. In the conventional edge-lit backlight module, these results indicate that the additional optical components, such as BEFs or diffusers, not only lead to energy loss, but also increase the leakage of light at the edge of the backlight module. However, in the high-efficiency backlight module, the crisscross LGP and diffuser replace the conventional edge-lit backlight module to reduce the number of optical components. Moreover, more light can reach receiver 5, meaning that the total system efficiency can be increased, as shown in Fig. 6(c).

D. Comparison between the High-efficiency and Conventional Edge-lit Backlight Module

Figures 7 and 8 show three-dimensional (3D) intensity charts for the conventional edge-lit backlight module and high-efficiency backlight module, respectively. The half-luminance angles of the conventional edge-lit backlight module and high-efficiency backlight module are 40 and 44 deg in the vertical direction, and 42 and 36 deg in the horizontal direction, respectively. These results demonstrate that the half-luminance angle is almost the same for both modules.

Since they contain no prism sheets, the energy loss of the high-efficiency backlight module is lower than for the conventional edge-lit backlight module. There is a twofold increase in the optical efficiency for the high-efficiency backlight module, as shown in Fig. 9. In the simulation, the luminance is normalized by the on-axis luminance of the conventional backlight

module. With the increase in the optical efficiency, the on-axis luminance doubles.

The results for the dependence of the luminance and the off-axis angle are plotted in Fig. 10. Compared with the conventional edge-lit backlight module, there is a twofold increase in the on-axis luminance of the high-efficiency backlight module. The FWHM of the high-efficiency backlight module is almost the same as that of the conventional edge-lit backlight module.

4. Tolerance Analysis

A. Contraposition Problem

The illumination uniformity of the high-efficiency backlight module can be controlled by the design of the top and bottom prism microstructures. However, a contraposition problem may occur due to the manufacturing alignment process, which will cause differences between the product and our design. Furthermore, this problem will affect the illumination uniformity. Thus, we must analyze the impact of the alignment of the microstructures on the resultant uniformity. In Fig. 11(a), the placement of microstructures is analyzed by separately shifting the top prism microstructures, the bottom prism microstructures and the trapezoidal microstructures. The placement of microstructures from −5 mm to +5 mm is simulated and variations in the illumination uniformity is observed.

Figure 11(b) shows the placement of microstructures and illumination uniformity under the nine-point measuring method. The maximum illumination uniformity is obtained at x at 0 mm. The variation of uniformity is slight for different placements of the microstructures; therefore we can say that the tolerance of the three-layer alignment is high. The illumination uniformity remains above 75% for the various placements of the microstructures from −5 mm to 5 mm. The placement of the

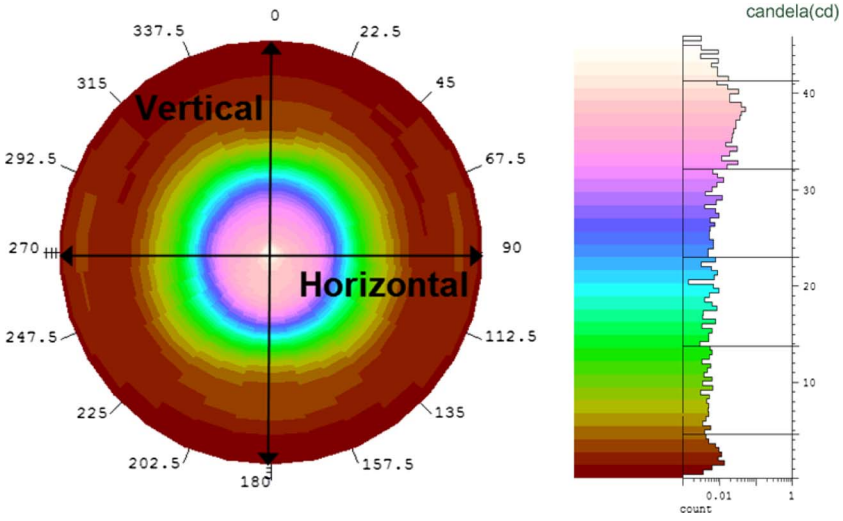

Fig. 7. 3D intensity chart for the conventional edge-lit backlight module.

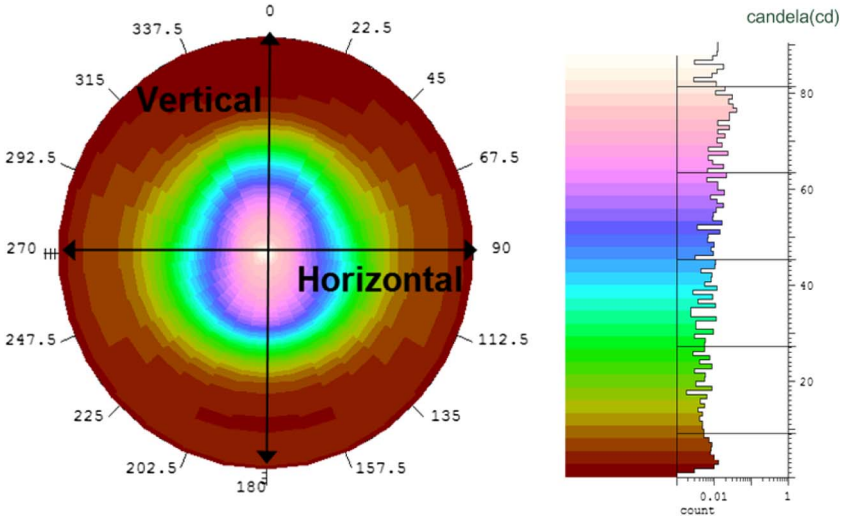

Fig. 8. 3D intensity chart for the high-efficiency backlight module.

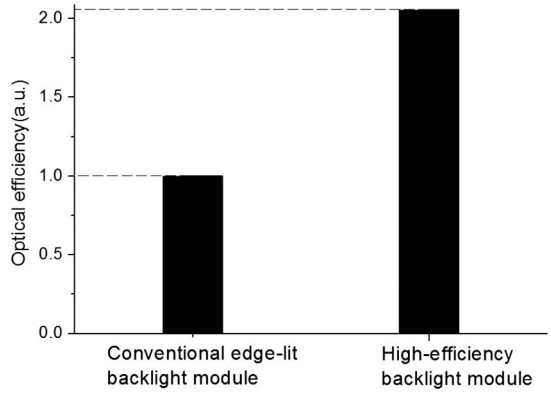

Fig. 9. Optical efficiency of the conventional edge-lit backlight module and the high-efficiency backlight module.

trapezoidal microstructures produces the slightest variation of illumination uniformity among the three kinds of microstructures, because the arrangement is perpendicular to that of the top prism microstructures and bottom prism microstructures.

B. Round Angle of the Prism Microstructures

In past studies, the draft angle of the bottom of the prism microstructures did not influence the performance of the backlight module [18]. Since our design used the same way to collimate the light in the vertical direction, it was unnecessary to analyze the tolerance for the draft angle of the bottom prism microstructures.

Considering that the LGP is designed based on flow-line theory, the round angle of the bottom microstructures can have a serious effect on the optical efficiency of the backlight module. In our design, the crisscross LGP has two guiding modes, based on the top prism microstructures of the LGP and the bottom prism microstructures of the OPF. The slanted angle of the LGP's top prism microstructures is designed by one degree, so the optical efficiency of the crisscross LGP will not be affected much by the round angle of the top prism microstructures. Thus,

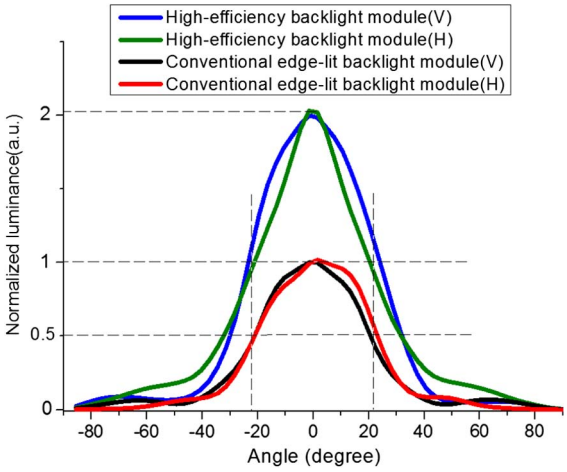

Fig. 10. Angular distributions for the conventional edge-lit backlight module and the high-efficiency backlight module.

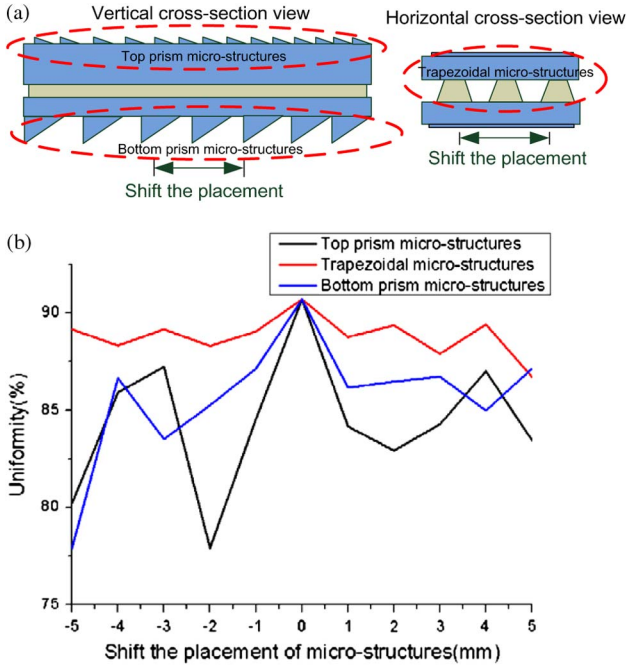

Fig. 11. Tolerance analysis for the contraposition problem: (a) shifted placement of microstructures and (b) relationship between uniformity and placement of the microstructures.

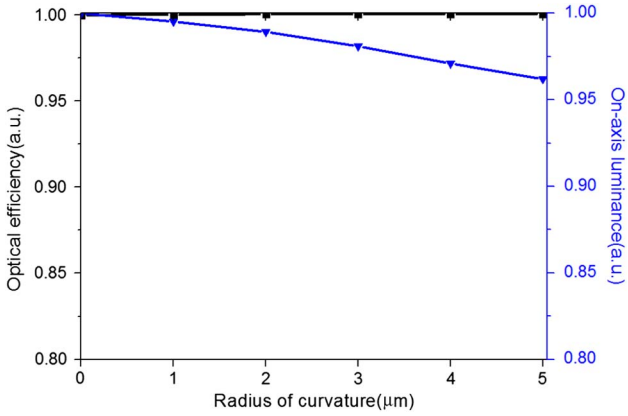

Fig. 12. Relationship between the round angles of the microstructures, normalized optical efficiency and normalized on-axis luminance.

we analyzed the round angles of the bottom prism microstructures. There is not much variation in the optical efficiency as the round angle of the bottom prism microstructures is increased, but there is a slight decrease in the on-axis luminance. Figure 12 shows the relationship between them. These results mean that the effect on the optical efficiency for this range of round angle is minimal.

5. Conclusion

In summary, we have presented a high-efficiency backlight module with a crisscross LGP and diffuser. Using this approach, we can increase both the optical efficiency and the on-axis luminance up to two times. In the vertical direction, the half-luminance angles of

the conventional edge-lit backlight module and high-efficiency backlight module are 40 and 44 deg; while in the horizontal direction they are 42 and 36 deg, respectively. The light field of the backlight module shows that two-dimensional collimation can be achieved by designing the slanted angles of the bottom prism microstructures and trapezoidal microstructures. Compared to the backlight module designed based on the flow-line method, the high-efficiency backlight module is simpler to implement and could also be used to reduce energy loss and the carbon footprint.

This study was supported in part by the National Science Council (Project Nos. NSC102-2220-E-009-006 and NSC101-2622-E-009-CC3) and in part by the "Aim for the Top University Plan" of the National Chiao Tung University and the Ministry of Education, Taiwan.

References

1. W. Zhang, H. Wang, L. Ji, and C. Liu, "Design and simulation of the LGP structure for LED backlight," Proc. SPIE **7655**, 765537 (2010).
2. T. Dekker, T. Bergman, and G. Vissenberg, "From backlight to Luminaire," SID Int. Symp. Dig. Tech. Pap. **43**, 248–251 (2012).
3. K. Käläntär, S. Matsumoto, and T. Onishi, "Functional light guide plate characterized by optical micro-deflector and micro-reflector for LCD backlight," IEICE Trans. Electron. **E84-C**, 1637–1646 (2001).
4. M. Anandan, "Progress of LED backlights for LCDs," J. Soc. Inf. Disp. **16**, 287–310 (2008).
5. S. Kobayashi, S. Mikoshiba, and S. Lim, *LCD Backlights* (Wiley, 2009).
6. K. Käläntär, "Modified functional light guide plate for backlighting transmissive LCDs," J. Soc. Inf. Disp. **11**, 641–645 (2003).
7. J. H. Lee, J. B. Yoon, J. Y. Choi, and J. B. Yoon, "A novel LCD backlight unit using a light guide plate with high fill-factor microlens array and a conical microlens array sheet," SID Int. Symp. Dig. Tech. Pap. **38**, 465–468 (2007).
8. O. Dross, W. A. Parkyn, J. Chaves, W. Falicoff, J. C. Miñano, P. Benitez, and R. Alvarez, "A superior architecture of brightness enhancement for display backlighting," Proc. SPIE **6338**, 63380G (2006).
9. J. C. Miñano, P. Benitez, J. Chaves, M. Hernandez, O. Dross, and A. Santamaria, "High-efficiency LED backlight optics designed with the flow-line method," Proc. SPIE **5942**, 594202 (2005).
10. D. Grabovičkić, P. Benítez, J. C. Miñano, and J. Chaves, "LED backlight designs with the flow-line method," Opt. Express **20**, A62–A68 (2012).
11. K. Fujisawa, I. Onishi, and Y. Fujiwara, "Edge-light backlight unit using optically patterned film," Jpn. J. Appl. Phys. **46**, 194–199 (2007).
12. A. Nagasawa and K. Fujisawa, "An ultra-slim backlight system using optical- patterned film," SID Int. Symp. Dig. Tech. Pap. **36**, 570–573 (2005).
13. American National Standards Institute (ANSI) IT7.215-1992, http://www.ansi.org.
14. Chi Mei Optoelectronics Corp., http://www.datasheet.in/datasheet-html/N/1/0/N101L6-L0B_CMIMEI.pdf.html.
15. 3M-Vikuiti™ ESR Film, http://www.pronatindustries.com/eng/catalogue.php?instance_id=2&actions=list&id=556.
16. KEIWA Inc., http://www.keiwa.co.jp/e/product/pdf_Folder/Opalus_E_200904.pdf.
17. TSUJIDEN CO. LTD., http://www.tsujiden.co.jp/eng/product/product_info_diffusion.html.
18. J. W. Pan and C. W. Fan, "High luminance hybrid light guide plate for backlight module application," Opt. Express **19**, 20079–20087 (2011).
19. D. Feng, Y. Yan, X. Yang, G. Jin, and S. Fan, "Novel integrated light guide plates for liquid crystal display backlight," J. Opt. A **7**, 111–117 (2005).
20. R. Winston, J. C. Miñano, and P. Benítez, *Nonimaging Optics*, (Academic, 2004).
21. A. Nagasawa, T. Eguchi, Y. Sanai, and K. Fujisawa, "Ultra-slim and bendable system with a unified component for liquid crystal display applications," Opt. Rev. **15**, 38–43 (2008).
22. P. A. Davies, "Edge-ray principle of nonimaging optics," J. Opt. Soc. Am. A **11**, 1256–1259 (1994).